PCCP

PAPER

View Article Online
View Journal | View Issue

Cite this: *Phys. Chem. Chem. Phys.*, 2016, **18**, 15081

Protonation induces base rotation of purine nucleotides pdGuo and pGuo†

R. R. Wu,[a] C. C. He,[a] L. A. Hamlow,[a] Y.-w. Nei,[a] G. Berden,[b] J. Oomens[bc] and M. T. Rodgers*[a]

Received 26th February 2016,
Accepted 3rd May 2016

DOI: 10.1039/c6cp01354f

www.rsc.org/pccp

Infrared multiple photon dissociation (IRMPD) action spectra of the protonated forms of 2′-deoxyguanosine-5′-monophosphate and guanosine-5′-monophosphate, $[pdGuo+H]^+$ and $[pGuo+H]^+$, are measured over the IR fingerprint and hydrogen-stretching regions using the FELIX free electron laser and an OPO/OPA laser system. Electronic structure calculations are performed to generate low-energy conformations of $[pdGuo+H]^+$ and $[pGuo+H]^+$ and determine their relative stabilities at the B3LYP/6-311+G(2d,2p)//B3LYP/6-311+G(d,p) and MP2(full)/6-311+G(2d,2p)//B3LYP/6-311+G(d,p) levels of theory. Comparative analyses of the measured IRMPD action spectra and B3LYP/6-311+G(d,p) linear IR spectra computed for the low-energy conformers are performed to determine the most favorable site of protonation and the conformers present in the experiments. These comparisons and the computed energetics find that N7 protonation is considerably preferred over O6 and N3, and the N7 protonated ground-state conformers of $[pdGuo+H]^+$ and $[pGuo+H]^+$ are populated in the experiments. The 2′-hydroxyl substituent does not significantly impact the stable low-energy conformers of $[pdGuo+H]^+$ *vs.* those of $[pGuo+H]^+$. The effect of the 2′-hydroxyl substituent is primarily reflected in the relative intensities of the measured IRMPD bands, as the IRMPD profiles of $[pdGuo+H]^+$ and $[pGuo+H]^+$ are quite similar. Comparisons to previous IRMPD spectroscopy investigations of the protonated forms of the guanine nucleosides, $[dGuo+H]^+$ and $[Guo+H]^+$, and deprotonated forms of the guanine nucleotides, $[pdGuo-H]^-$ and $[pGuo-H]^-$, provide insight into the effects of the phosphate moiety and protonation on the conformational features of the nucleobase and sugar moieties. Protonation is found to induce base rotation of the guanine residue to an *anti* orientation *vs.* the *syn* orientation found for the deprotonated forms of the guanine nucleotides.

Introduction

The nucleobase, sugar and phosphate moieties that comprise DNA and RNA nucleotide polymers possess various hydrogen-bond donors and acceptors that provide opportunities for a wide variety of intra- and intermolecular hydrogen-bonding interactions to occur in these systems. Therefore, hydrogen-bonding interactions generally play a significant role in determining the overall three-dimensional structures exhibited by macromolecular DNA and RNA.[1] Variations in the hydrogen-bonding interactions present in DNA and RNA lead to changes in their structures that influence their biological functions. In particular, protonation greatly influences the canonical hydrogen-bonding interactions.[2–5] Therefore, protonation contributes to a number of novel nucleic acid structures, such as triple stranded DNA and i-motif tetramers.[6,7]

As canonical DNA and RNA nucleotides, guanine nucleotides participate in a variety of unique biological processes. For example, the hydrogen-bond donors and acceptors of the guanine nucleobase facilitate self-assembly of G-quadruplexes, which are major contributors to telomeric DNA and are being investigated as novel anticancer targets.[8,9] Guanine nucleotides provide multiple favorable binding sites for bare alkali, alkaline earth, and transition metal cations,[10–14] as well as metal-containing chemotherapeutic drugs such as cisplatin.[15,16] As a result, guanine nucleotides have been widely studied.[17–26] However, studies of the intrinsic properties of isolated guanine mononucleotides in the gas phase, free from the influence of solvent effects and interactions with other ions and molecules, are still rather limited.[27–30] Thus far, the deprotonated guanine

[a] *Department of Chemistry, Wayne State University, Detroit, Michigan 48202, USA. E-mail: mrodgers@chem.wayne.edu*
[b] *FELIX Laboratory, Institute for Molecules and Materials, Radboud University, Toernooiveld 7c, 6525 ED, Nijmegen, The Netherlands*
[c] *van't Hoff Institute for Molecular Sciences, University of Amsterdam, 1090 GD, Amsterdam, The Netherlands*

† Electronic supplementary information (ESI) available: Structures of the B3LYP/6-311+G(d,p) low-energy conformers of $[pdGuo+H]^+$ and $[pGuo+H]^+$ and their relative Gibbs free energies at 298 K calculated at B3LYP/6-311+G(2d,2p) and MP2(full)/6-311+G(2d,2p) levels of theory. Comparisons of the measured IRMPD spectra and calculated IR spectra of select low-energy conformers of $[pdGuo+H]^+$ and $[pGuo+H]^+$. See DOI: 10.1039/c6cp01354f

mononucleotides have received the most attention because the phosphate moieties of nucleic acids are deprotonated under physiological conditions.[1] Nei *et al.*[29,30] found that among the deprotonated forms of the canonical DNA and RNA mononucleotides, the deprotonated guanine mononucleotides, $[pdGuo–H]^-$ and $[pGuo–H]^-$, distinguish themselves from the others because they exhibit *syn* nucleobase orientations that are stabilized by a strong ionic hydrogen-bonding interaction between the 2-amino hydrogen atom of guanine and one of the oxygen atoms of the deprotonated phosphate moiety. This structural difference also explains the collision activation dissociation (CAD) behavior of $[pdGuo–H]^-$ in an ion trap mass spectrometer that is notably different from the other deprotonated DNA mononucleotides examined, as it is exceptionally stable toward decomposition *via* loss of the neutral nucleobase.[27] In spite of the importance and uniqueness of the deprotonated guanine mononucleotides, protonation may ultimately alter the local or overall structures of nucleic acids as a result of changes in the hydrogen-bonding network. Therefore, it is also of interest to study the intrinsic properties of the protonated guanine mononucleotides to determine the most favorable site of protonation, preferred hydrogen-bonding patterns, and features of their low-energy conformations. The knowledge gained may provide insight into the structures and biochemical properties of guanine nucleotides in a low pH environment.

Gidden *et al.* performed ion mobility mass spectrometry (IM-MS) and computational studies to characterize the gas-phase conformations of the deprotonated and protonated forms of pdGuo.[28] Their study suggested that a family of conformations of $[pdGuo–H]^-$ where guanine exhibits a *syn* orientation and the sugar is C3′-*endo* puckered are present in the experiments. In contrast, upon protonation guanine rotates to an *anti* orientation and the sugar puckering switches to C2′-*endo*. Their results for $[pdGuo–H]^-$ were later further validated by Nei *et al.* who used infrared multiple photon dissociation (IRMPD) action spectroscopy and synergistic computations to characterize the gas phase conformations of the DNA mononucleotides.[29] Thus, the IM-MS results indicate that protonation has a significant impact on the structure of pdGuo, and induces changes in both the nucleobase orientation and sugar puckering.

Like IM-MS, IRMPD action spectroscopy experiments combined with theoretical calculations have proven to be a very robust approach for examining the gas-phase intrinsic properties of biologically relevant ions[31–35] and in particular have been employed to investigate guanine nucleosides and nucleotides in various states of ionization and complexation.[14,16,26,29,30,33] In particular, we have examined the gas-phase conformations and energetics of the protonated forms of 2′-deoxyguanosine and guanosine, $[dGuo+H]^+$ and $[Guo+H]^+$,[33] as well as deprotonated forms of pdGuo and pGuo, $[pdGuo–H]^-$ and $[pGuo–H]^-$,[29,30] using IRMPD spectroscopy assisted by theoretical calculations. In the current work, we extend our studies to include the protonated forms of pdGuo and pGuo, $[pdGuo+H]^+$ and $[pGuo+H]^+$, using the IRMPD action spectroscopy and theoretical calculations approach to characterize the gas-phase conformations and energetics of these systems. Comparisons among all of these systems, $[dGuo+H]^+$, $[Guo+H]^+$, $[pdGuo–H]^-$, $[pGuo–H]^-$, $[pdGuo+H]^+$ and $[pGuo+H]^+$, enables the influence of the state of ionization (deprotonation *vs.* protonation), the 2′-hydroxyl substituent, and the guanine nucleobase, sugar and phosphate moieties on the structure and stability of these systems to be elucidated. Furthermore, comparisons to results from the earlier IM-MS study also provide validation of the conclusions regarding the structures of the guanine nucleotides and how they are influenced by protonation.

Experimental and computational methods

IRMPD spectroscopy experimental setup

A Fourier transform ion cyclotron resonance mass spectrometer (FT-ICR MS)[36–38] equipped with a 4.7 T superconducting magnet and coupled to a widely-tunable free electron laser (FEL)[39] or an OPO/OPA laser system was used to acquire IRMPD action spectra of $[pdGuo+H]^+$ and $[pGuo+H]^+$ over the IR fingerprint and hydrogen-stretching regions. The guanine nucleotides, pdGuo and pGuo, were purchased from Sigma-Aldrich. Approximately 1 mM pdGuo or pGuo and 100 mM acetic acid or 10 mM HCl were dissolved in 50% : 50% MeOH/H_2O solutions. The solutions were delivered to a Micromass "Z-spray" electrospray ionization (ESI) source at a flow rate of $\sim$4.5–6.0 μL min^{-1}. Ions emanating from the ESI source were collected in an rf hexapole ion trap for several seconds to affect efficient thermalization of the ions, and then pulse extracted through a quadrupole bender. The ions traveled through a 1 m long rf octopole ion guide into the FT-ICR MS and were stored in the ICR cell to cool to room temperature by radiative emission.[37] $[pdGuo+H]^+$ and $[pGuo+H]^+$ ions were isolated using stored waveform inverse Fourier transform (SWIFT) techniques and irradiated for 1.5–3 s by the FEL (10 pulses per s with 15–50 mJ per pulse) or 3–4 s by the OPO/OPA laser system (10 pulses per s with 10–20 mJ per pulse) to induce IR photodissociation over the IR fingerprint and hydrogen-stretching regions, respectively.

Theoretical calculations

The chemical structures of neutral pdGuo and pGuo are displayed in Fig. 1. All favorable protonation sites were investigated and include N3, O6, N7 and the phosphate oxo oxygen atom. 300 candidate structures for each site of protonation were generated by simulated annealing using HyperChem software[40] with the Amber 2 force field. The simulated annealing procedure employed in these studies parallels that described in detail previously.[31–33] Geometry optimizations, frequency analyses, and single point energy calculations of 20–30 candidate structures for each protonation site were performed using the Gaussian 09 suite of programs.[41] All candidate structures were first optimized at the B3LYP/6-31G(d) level of theory to facilitate convergence, and then re-optimized using a larger basis set, 6-311+G(d,p), to improve the description of the intramolecular hydrogen-bonding interactions. Frequency analyses were also performed using the B3LYP/6-311+G(d,p) basis set to generate calculated

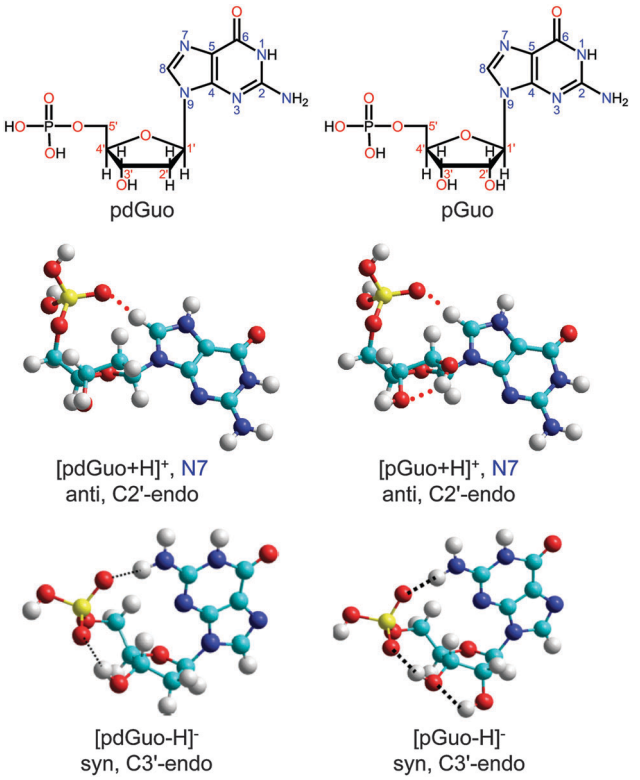

Fig. 1 Chemical structures of neutral pdGuo and pGuo. The numbering of the nucleobase and sugar moieties is also shown. The ground-state conformers of $[pdGuo+H]^+$ and $[pGuo+H]^+$ predicted at the B3LYP/6-311+G(2d,2p)//B3LYP/6-311+G(d,p) and MP2(full)/6-311+G(2d,2p)//B3LYP/6-311+G(d,p) levels of theory. The ground-state conformers of $[pdGuo-H]^-$ and $[pGuo-H]^-$ are also shown for comparison and are taken from ref. 29 and 30, respectively. The site of protonation, nucleobase orientation, and sugar puckering are also indicated for each protonated nucleotide.

IR spectra. Single point energies were calculated at the B3LYP and MP2(full) levels of theory using the 6-311+G(2d,2p) basis set including zero-point energy (ZPE) and thermal corrections to 298 K. Due to anharmonicity of the vibrational modes of the phosphate moiety, scaling factors between 0.98 and 1.07 are needed to bring the computed frequencies into agreement with measured values.[14,16,29,30,42–46] In this work, a factor of 1.03 is applied to the frequencies below $\sim$1350 cm^{-1} (shown in red in the calculated spectra) to best reproduce the measured bands associated with the phosphate moiety. A factor of 0.986 is applied to the frequencies above $\sim$1350 cm^{-1} in the IR fingerprint region (shown in blue), and a factor of 0.956 is used for the hydrogen-stretching region (shown in green). In addition, the calculated vibrational transitions are broadened using a 20 cm^{-1} fwhm Gaussian line shape for the IR fingerprint region, and 15 cm^{-1} broadening for the hydrogen-stretching region, to reproduce the shapes of the measured IRMPD profiles.

Results

IRMPD action spectroscopy

The FELIX free electron laser and an OPO/OPA laser system were used to induce photodissociation of $[pdGuo+H]^+$ and $[pGuo+H]^+$

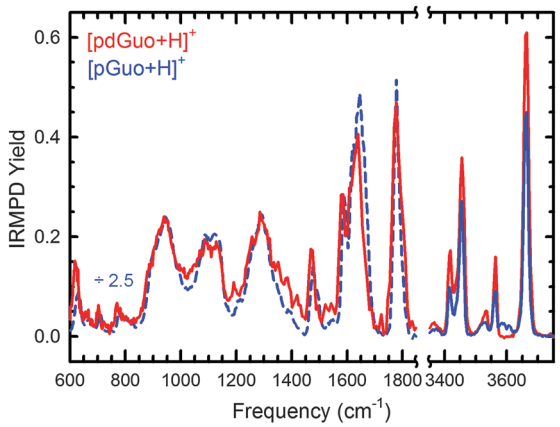

Fig. 2 Infrared multiple photon dissociation (IRMPD) action spectra of $[pdGuo+H]^+$ and $[pGuo+H]^+$ in the IR fingerprint and hydrogen-stretching regions. The IRMPD yield of $[pGuo+H]^+$ has been divided by a factor of 2.5 (and shown as a dashed line) in the IR fingerprint region to facilitate comparisons.

to produce protonated guanine, $[Gua+H]^+$, as the primary ionic product detected. $[Gua+H-H_2O]^+$ was also observed as a minor product in the photodissociation of $[pdGuo+H]^+$ when induced by the FELIX free electron laser. The ratio of the total product ion intensity and that of the protonated mononucleotide, $[pNuo+H]^+$ = $[pdGuo+H]^+$ or $[pGuo+H]^+$, determines the IRMPD yield at each frequency of irradiation according to eqn (1),

$$\text{IRMPD yield} = \sum_i I_{\text{product}_i} \Big/ \left(\sum_i I_{\text{product}_i} + I_{[\text{pNuo+H}]^+} \right) \quad (1)$$

The IRMPD yield was corrected for variations in the laser power as a function of the wavelength of the free electron or OPO lasers using linear scaling. IRMPD action spectra of $[pdGuo+H]^+$ and $[pGuo+H]^+$ were measured over the ranges extending from $\sim$550 to 1900 cm^{-1} and $\sim$3300 to 3800 cm^{-1} and are compared in Fig. 2. The IRMPD spectral profiles of $[pdGuo+H]^+$ and $[pGuo+H]^+$ are remarkably similar in both regions. However, $[pGuo+H]^+$ exhibits higher IRMPD yield (by a factor of $\sim$2.5) than $[dGuo+H]^+$ in the fingerprint region, whereas in the hydrogen-stretching region, $[pdGuo+H]^+$ produces $\sim$30% higher yield than $[pGuo+H]^+$. These differences in the IRMPD band intensities observed for $[pdGuo+H]^+$ and $[pGuo+H]^+$ are explained based on differences in the intramolecular hydrogen-bonding interactions associated with the 2′-hydroxyl substituent.

Theoretical results

The B3LYP/6-311+G(2d,2p)//B3LYP/6-311+G(d,p) and MP2(full)/6-311+G(2d,2p)//B3LYP/6-311+G(d,p) levels of theory predict the same ground-state conformers for $[pdGuo+H]^+$ and $[pGuo+H]^+$, which are shown in Fig. 1. N7 is the most favorable site of protonation for both $[pdGuo+H]^+$ and $[pGuo+H]^+$, consistent with that found for their analogous nucleosides, $[dGuo+H]^+$ and $[Guo+H]^+$.[33] In the ground-state conformers of these species, guanine takes on an *anti*-orientation relative to the glycosidic bond, again parallel to that found for $[dGuo+H]^+$ and $[Guo+H]^+$. The sugar moiety exhibits C2′-*endo* puckering, in contrast to

Table 1 Key geometrical parameters of the ground-state conformers of protonated guanine nucleosides and nucleotides

	Bond distances (Å)		Dihedral angles (°)		
Species	C1′–N9	C8H···O	∠C4N9C1′C2′	∠C1′C2C3′C4′	∠O5′C5′C4′O4′
$[pdGuo+H]^+$	1.471	1.848	108.8	−27.1	−72.9
$[pGuo+H]^+$	1.464	1.858	110.7	−28.6	−74.9
$[dGuo+H]^+$ [a]	1.508	2.075	84.6	31.0	−62.6
$[Guo+H]^+$ [a]	1.498	2.117	84.8	31.0	−62.9

[a] Values taken from ref. 33.

that found for $[dGuo+H]^+$ and $[Guo+H]^+$,[33] which both exhibit C3′-*endo* puckering. Again parallel to that found for $[dGuo+H]^+$ and $[Guo+H]^+$,[33] the 2′-hydroxyl substituent does not exert a significant influence on the conformational features of the ground-state structure of $[pGuo+H]^+$ as compared to those of $[pdGuo+H]^+$. Key geometrical parameters of the ground-state conformers of $[pdGuo+H]^+$ and $[pGuo+H]^+$ are compared with those found for $[dGuo+H]^+$ and $[Guo+H]^+$ in Table 1.[33] The RNA nucleosides and nucleotides exhibit slightly shorter glycosidic bonds than their DNA analogues, suggesting that the 2′-hydroxyl substituent stabilizes the glycosidic bond. The phosphate oxo oxygen atoms of $[pdGuo+H]^+$ and $[pGuo+H]^+$ enable a stronger C8H···O═P intramolecular non-canonical hydrogen-bonding interaction than that of the C8H···O5′ interaction in their nucleoside analogues. The presence of the phosphate moiety in $[pdGuo+H]^+$ and $[pGuo+H]^+$ slightly alters the orientations of the nucleobase and 5′-substituent relative to the sugar moiety as compared to those in $[dGuo+H]^+$ and $[Guo+H]^+$. Moreover, the sugar puckering of $[pdGuo+H]^+$ and $[pGuo+H]^+$ clearly differs from that of $[dGuo+H]^+$ and $[Guo+H]^+$.[33]

Table 2 lists the relative enthalpies and Gibbs free energies at 0 and 298 K of the low-energy conformers of $[pdGuo+H]^+$ and $[pGuo+H]^+$ for N7, N3 and O6 protonation sites. These low-energy conformers along with their relative free energies at 298 K computed at both the B3LYP and MP2(full) levels of theory are shown in Fig. S1 and S2 of the ESI.† The low-energy conformers chosen for display include all combinations of the favorable protonation sites, nucleobase orientations, and sugar puckering. In all cases, initial structures involving protonation of the phosphate moiety always converged to N7 protonated species. The nomenclature chosen to differentiate the various stable conformers found is based on the sites of protonation followed by a capital letter when highly parallel conformers are found for both $[pdGuo+H]^+$ and $[pGuo+H]^+$. Unique conformations are found for $[pdGuo+H]^+$ and $[pGuo+H]^+$ that result from the absence or presence of the 2′-hydroxyl substituent, respectively. Thus, a lowercase letter is used for conformers that are found only for $[pdGuo+H]^+$ (**N3a**), whereas a lowercase Roman numeral is used for conformers that are found only for $[pGuo+H]^+$ (**N7i**, **N7ii**, **N7iii** and **N3i**). The N3 and O6 protonated conformers are predicted to be >30 kJ mol^{-1} higher in free energy than the N7 protonated ground-state conformers.

Table 2 Relative enthalpies and free energies at 0 and 298 K in kJ mol^{-1} of the stable low-energy conformers of $[pdGuo+H]^+$ and $[pGuo+H]^+$ [a]

		B3LYP			MP2(full)		
Species	Conformer	ΔH_0	ΔH_{298}	ΔG_{298}	ΔH_0	ΔH_{298}	ΔG_{298}
$[pdGuo+H]^+$	**N7A**	**0.0**	**0.0**	**0.0**	**0.6**	**2.6**	**0.0**
	N7B	2.1	1.8	2.2	4.7	6.3	4.2
	N7C	8.4	6.4	13.5	0.0	0.0	4.5
	N7D	12.0	10.8	13.7	0.7	1.5	1.8
	N3A	27.6	25.7	32.5	12.7	12.8	16.9
	O6A	43.3	41.7	45.7	36.1	36.4	37.9
	O6B	49.8	49.9	50.0	47.9	50.0	47.5
	N3a	97.5	98.5	95.7	88.1	91.1	85.7
$[pGuo+H]^+$	**N7A**	**0.0**	**0.0**	**0.0**	**0.2**	**3.8**	**0.0**
	N7B	2.2	1.1	4.9	3.7	4.8	4.8
	N7i	4.4	4.4	5.0	3.7	5.8	2.7
	N7ii	8.5	8.1	10.1	9.7	11.5	9.8
	N7iii	9.8	8.8	11.4	3.3	4.5	3.4
	N7C	6.7	4.4	12.9	0.0	0.0	4.7
	N7D	11.6	10.1	14.6	0.6	1.3	2.1
	N3A	33.3	31.2	37.6	20.6	20.7	23.4
	O6A	42.0	40.5	44.9	36.7	37.4	38.0
	O6B	47.6	47.7	47.9	47.5	50.0	46.3
	N3i	65.4	64.7	68.4	42.2	43.8	43.7

[a] Single point energy calculations using the B3LYP/6-311+G(d,p) optimized structures are performed at the B3LYP/6-311+G(2d,2p) and MP2(full)/6-311+G(2d,2p) levels of theory and include ZPE and thermal corrections.

N7 protonation

$[pdGuo+H]^+$ and $[pGuo+H]^+$ prefer the *anti* nucleobase orientation and C2′-*endo* sugar puckering as found in their ground-state conformations shown in Fig. 1. Based on the relative stabilities of the *anti* conformers, **N7A**, **N7B**, **N7i** and **N7ii** of $[pGuo+H]^+$, the structures are more stable when the 2′-hydroxyl substituent serves as a hydrogen-bond donor (**N7A** and **N7B**). The *anti* conformers are calculated to be >10 kJ mol^{-1} (B3LYP) more stable than the *syn* conformers. The **N7D** conformers of both $[pdGuo+H]^+$ and $[pGuo+H]^+$ have noncanonical C8H···O5′ and canonical O3′H···O═P hydrogen bonds between the *anti*-oriented nucleobase, sugar, and phosphate moieties, respectively. However, these intramolecular hydrogen-bonding interactions confine the conformations to less desirable nucleobase and phosphate orientations and sugar puckering, which destabilize the **N7D** conformers relative to the **N7A** conformers. Differences in stability among the N7 protonated conformers are much smaller for MP2(full) calculations, where most lie within 5 kJ mol^{-1} of the ground-state conformers.

N3 and O6 protonation

N3 protonation is preferred over O6, in contrast to that found for $[dGuo+H]^+$ and $[Guo+H]^+$.[33] N3 and O6 protonated conformers of both $[pdGuo+H]^+$ and $[pGuo+H]^+$ are found to be >30 kJ mol^{-1} (B3LYP) and >15 kJ mol^{-1} (MP2(full)) less stable than the most

stable N7 protonated conformers. Both the N3 and O6 protonated conformers of $[pdGuo+H]^+$ and $[pGuo+H]^+$ exhibit energetic preferences for a *syn* orientation of the nucleobase and C2′-*endo* sugar puckering rather than an *anti* orientation with C2′-*endo* sugar puckering as found for N7 protonation.

Discussion

Elucidation of conformations of $[pdGuo+H]^+$ populated in the experiments

The measured IRMPD and predicted IR spectra of the ground-state and most stable low-energy conformers for each favorable site of protonation, **N7A**, **N7C**, **N3A** and **O6A** of $[pdGuo+H]^+$ are compared in Fig. 3 over the IR fingerprint and hydrogen-stretching regions. The IR spectrum predicted for the ground-state conformer, **N7A**, exhibits excellent agreement with the measured IRMPD spectrum except for the weak and broad band that appears at 3535 cm^{-1}, which is not predicted by theory. This unexpected feature may be attributed to an overtone of the strong IR band measured at 1770 cm^{-1}. In contrast, the calculated IR spectra of **N7C**, **N3A** and **O6A** exhibit obvious discrepancies with the measured IRMPD spectrum above 1500 cm^{-1} that are highlighted in the figure. In the IR fingerprint region, the bands predicted at 1675 and 1615 cm^{-1} for **N7C**, and 1705 and 1630 cm^{-1} for **O6A**, are higher in frequency than the measured bands at 1639 and 1578 cm^{-1}, respectively. The bands predicted at 1825 and 1695 cm^{-1} for **N3A** are also higher in frequency than the bands observed at 1770 and 1639 cm^{-1}. In the hydrogen-stretching region, the bands predicted at 3655, 3645 and 3650 cm^{-1} for **N7C**, **N3A** and **O6A**, respectively, are all lower in frequency than the measured band at 3661 cm^{-1}. The band at 3580 cm^{-1} predicted for **O6A** is higher in frequency than the band observed at 3564 cm^{-1}. The bands predicted at 3510, 3490 and 3505 cm^{-1} for **N7C**, **N3A**, and **O6A**, respectively, are not observed in the measured spectrum. The band predicted at 3440 cm^{-1} for **N7C** is lower in frequency than the band observed at 3455 cm^{-1}. Therefore, among these conformers only the ground-state conformer, **N7A**, is populated in the experiments. The N3 and O6 protonated conformers clearly do not contribute to the measured spectrum. The measured IRMPD and calculated IR spectra of the **N7B**, **N7D**, **O6B** and **N3a** of $[pdGuo+H]^+$ are compared over the IR fingerprint and hydrogen-stretching regions in Fig. S3 of the ESI.† The IR spectra predicted for these conformers all exhibit distinctive differences from the measured IRMPD spectrum, indicating that they are not populated by ESI. A more detailed discussion is provided in the ESI.†

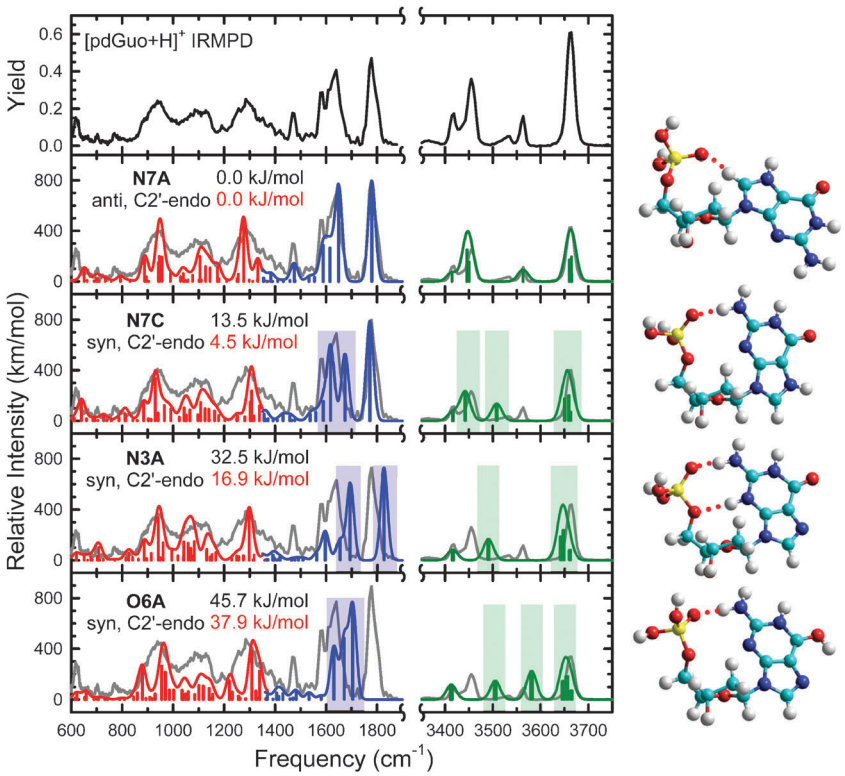

Fig. 3 Comparison of the measured IRMPD action spectrum of $[pdGuo+H]^+$ with the calculated IR spectra of the ground-state and most stable conformers for each protonation site of $[pdGuo+H]^+$ and the corresponding B3LYP/6-311+G(d,p) optimized structures. Also shown are the B3LYP/6-311+G(2d,2p) (in black) and MP2(full)/6-311+G(2d,2p) (in red) relative Gibbs free energies at 298 K. The site of protonation, nucleobase orientation and sugar puckering are also indicated for each conformer. To facilitate comparison of the measured and calculated spectra, the IRMPD spectrum is overlaid (in grey) with each calculated spectrum and scaled to match the intensity of the most intense feature in each region. Regions exhibiting obvious discrepancies between the measured and computed IR features are highlighted.

Table 3 Vibrational mode assignments for $[pdGuo+H]^+$ and $[pGuo+H]^+$ [a]

Vibrational mode assignment	Frequency (cm^{-1}) $[pdGuo+H]^+$	$[pGuo+H]^+$
P–OH bending	934	940
C5′–O5′, C4′–C5′, and sugar ring stretching	1106	1110
P═O stretching	1285	1283
N7–H in-plane bending	1468	1476
Nucleobase ring stretching	1578	1589
NH_2 scissoring	1639	1646
C═O stretching	1770	1776
N1–H stretching	3414	3410
NH_2 symmetric and N7–H stretching	3455	3451
Overtone of C═O stretching	3535	3535
NH_2 asymmetric and O2′H ($[pGuo+H]^+$) stretching	3564	3560
P–OH and O3′H stretching	3661	3661

[a] Vibrational assignments based on comparison of the measured IRMPD and calculated IR spectra of the ground-state **N7A** conformers of $[pdGuo+H]^+$ and $[pGuo+H]^+$.

In summary, comparative analyses of the measured IRMPD and IR spectra predicted for the stable structures computed for $[pdGuo+H]^+$ indicate that only a single conformer, the ground-state N7 protonated conformer, **N7A**, is populated in the experiments. Vibrational mode assignments of $[pdGuo+H]^+$ are interpreted based on the calculated IR spectrum of the **N7A** conformer, and are summarized in Table 3.

Elucidation of conformations of $[pGuo+H]^+$ populated in the experiments

The measured IRMPD and IR spectra computed for the ground-state and most stable low-energy conformers for each favorable site of protonation, **N7A**, **N7C**, **N3A** and **O6A** of $[pGuo+H]^+$ are compared in Fig. 4 over the IR fingerprint and hydrogen-stretching regions. Similar to that found for $[pdGuo+H]^+$, the calculated IR spectrum of the ground-state conformer, **N7A**, exhibits excellent agreement with the measured IRMPD spectrum except for the very weak and broad band observed at 3535 cm^{-1}, which is again not predicted by theory. As before, we attribute this band to an overtone of the strong IR band measured at 1776 cm^{-1}. Moreover, the calculated IR feature at 3685 cm^{-1}, arising from the hydrogen-bond acceptor O3′H stretching, is slightly shifted relative to the band measured at 3661 cm^{-1}. This shift is due to the anharmonicity of the hydrogen-bonding interaction between the two hydroxyls of the sugar moiety. Therefore, this feature is not diagnostic. Similarly, the hydrogen-bond acceptor O3′H stretches predicted at ~3685 cm^{-1} for the **N7C**, **N3A** and **O6A** are not diagnostic. However, other discrepancies between the measured IRMPD and IR spectra predicted for **N7C**, **N3A** and **O6A** are evident (see highlighted regions in Fig. 4) and sufficient to eliminate them from the experimental population. In the IR fingerprint region above 1500 cm^{-1}, the bands predicted at 1675 and 1620 cm^{-1} for **N7C**, and 1705 and

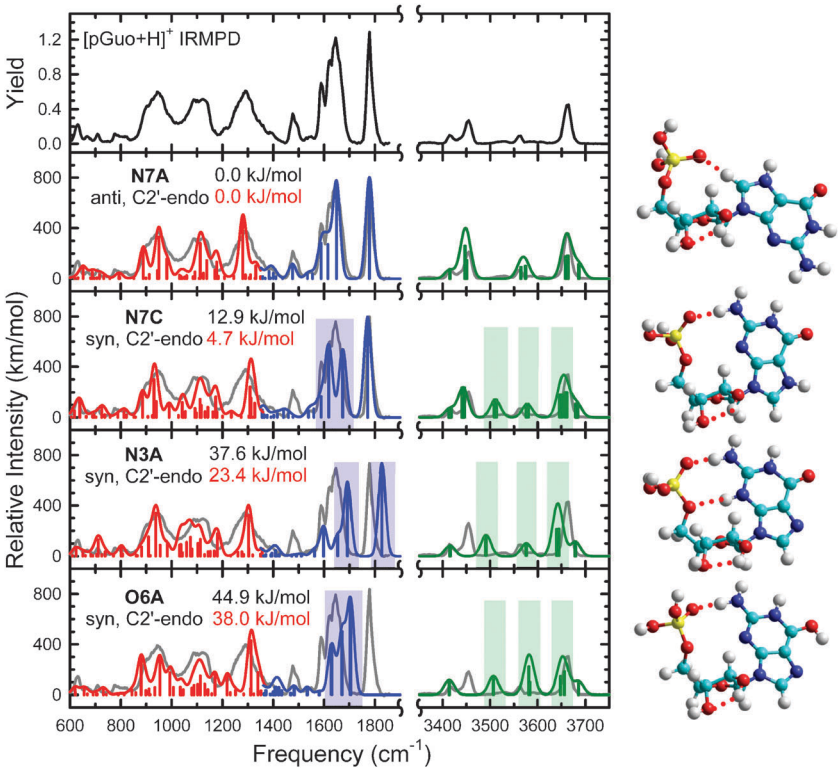

Fig. 4 Comparison of the measured IRMPD action spectrum of $[pGuo+H]^+$ with the calculated IR spectra of the ground-state and most stable conformers for each protonation site of $[pGuo+H]^+$ and the corresponding B3LYP/6-311+G(d,p) optimized structures. Also shown are the B3LYP/6-311+G(2d,2p) (in black) and MP2(full)/6-311+G(2d,2p) (in red) relative Gibbs free energies at 298 K. The site of protonation, nucleobase orientation and sugar puckering are also indicated for each conformer. To facilitate comparison of the measured and calculated spectra, the IRMPD spectrum is overlaid (in grey) with each calculated spectrum and scaled to match the intensity of the most intense feature in each region. Regions exhibiting obvious discrepancies between the measured and computed IR features are highlighted.

1630 cm^{-1} for **O6A** are higher in frequency than the measured bands at 1646 and 1589 cm^{-1}, respectively. The calculated bands at 1830 and 1690 cm^{-1} for **N3A** are also higher in frequency than the bands observed at 1776 and 1646 cm^{-1}, respectively. In the hydrogen-stretching region, the bands predicted at 3655, 3640 and 3650 cm^{-1} for **N7C**, **N3A** and **O6A**, respectively, are slightly lower in frequency than the measured band at 3661 cm^{-1}, whereas the calculated bands at 3580, 3575 and 3580 cm^{-1} for **N7C**, **N3A** and **O6A**, respectively, are slightly higher in frequency than the measured band at 3560 cm^{-1}. The calculated bands at 3510, 3490 and 3505 cm^{-1} for **N7C**, **N3A** and **O6A**, respectively, are not observed in the measured spectrum. Therefore, among these conformers, only the ground-state conformer, **N7A**, is populated in the experiments. The measured IRMPD and calculated IR spectra of the other low-energy conformers found for $[pGuo+H]^+$ are compared over the IR fingerprint and hydrogen-stretching regions in Fig. S4 and S5 of the ESI.† These comparisons clearly indicate the absence of these conformers in the experimental population. A more detailed discussion is provided in the ESI.†

In summary, similar to $[pdGuo+H]^+$, comparative analyses of the measured and calculated IR spectra of $[pGuo+H]^+$ indicates that only the ground-state N7 protonated conformer, **N7A**, is populated in the experiments. Significant differences between the measured IRMPD and calculated IR spectra for the N3 and O6 protonated conformers definitively rule out their presence in the experimental population. Vibrational mode assignments of the measured IRMPD spectral features are based on the calculated vibrational modes of **N7A** and are summarized in Table 3.

Comparison of IRMPD spectra of $[pdGuo+H]^+$ and $[pGuo+H]^+$

The measured IRMPD spectra of $[pdGuo+H]^+$ and $[pGuo+H]^+$ compared in Fig. 2 exhibit marked similarities indicating that the 2′-hydroxyl substituent does not significantly impact the IRMPD profiles. However, the 2′-hydroxyl substituent clearly exerts an evident influence on the IRMPD yields. The hydrogen-bonding interaction between the 2′- and 3′-hydroxyl substituents stabilizes and stiffens the sugar moiety, and leads to greater conformational flexibility of the nucleobase and phosphate moieties. As a result, intramolecular vibrational redistribution (IVR)[47,48] is more efficient and hence the IRMPD yield in the IR fingerprint region of $[pGuo+H]^+$ is more than ~2.5 times that of $[pdGuo+H]^+$. Conversely, flexible hydrogen-stretching arising from the free 3′-hydroxyl substituent of $[pdGuo+H]^+$ leads to a slightly higher IRMPD yield for $[pdGuo+H]^+$ than $[pGuo+H]^+$ in the hydrogen-stretching region. The effect of the 2′-hydroxyl substituent on the IRMPD yields is clearly an effect associated with the multiple photon nature of the experiments as the calculated IR intensities are virtually identical for the analogous conformers of $[pdGuo+H]^+$ and $[pGuo+H]^+$ (compare Fig. 3 *vs.* 4 as well as Fig. S3 *vs.* S4 and S5 of the ESI†).

Influence of the phosphate moiety

Consistent with those found for $[dGuo+H]^+$ and $[Guo+H]^+$,[33] the preferred gas-phase conformations of $[pdGuo+H]^+$ and $[pGuo+H]^+$ involve N7 protonation of the guanine nucleobase, which exists in an *anti* orientation. However, both $[dGuo+H]^+$ and $[Guo+H]^+$ prefer C3′-*endo* sugar puckering, whereas $[pdGuo+H]^+$ and $[pGuo+H]^+$ prefer C2′-*endo* puckering. Thus, the presence of the phosphate moiety induces a change in the sugar configuration. Similar to $[dGuo+H]^+$ and $[Guo+H]^+$, only N7 protonated *anti*-oriented low-energy conformers of $[pdGuo+H]^+$ and $[pGuo+H]^+$ are populated, whereas the N3 and O6 protonated conformers lie much higher in free energy and are not populated in the experiments. However, for $[dGuo+H]^+$ and $[Guo+H]^+$, multiple N7 protonated *anti*-oriented conformers are found to contribute to the experimental population, including both C3′-*endo* (ground-state conformers) and C2′-*endo* low-energy excited conformers. For $[Guo+H]^+$ in particular, the 2′- and 3′-hydroxyls adopt several orientations such that multiple rotamers exist among the low-energy conformers populated. In contrast, for $[pdGuo+H]^+$ and $[pGuo+H]^+$, the N7 protonated, *anti*-oriented, and C2′-*endo* sugar puckered ground-state conformers are exclusively populated in the experiments. For $[pGuo+H]^+$, both the 2′- and 3′-hydroxyls point down and away from the nucleobase and the 2′-hydroxyl serves as a hydrogen-bond acceptor in the O2′H···O3′ hydrogen-bonding interaction. Thus, interactions with the phosphate moiety stabilize the nucleobase and sugar moieties and largely constrain the flexibility of the gas-phase conformations, and lead to only a single conformation being populated in the experiments.

Protonation induced base rotation

The gas-phase conformations and energetics of the deprotonated guanine mononucleotides, $[pdGuo–H]^-$ and $[pGuo–H]^-$ have previously been examined by IRMPD spectroscopy and theory.[29,30] These studies found that in the ground-state structures of both $[pdGuo–H]^-$ and $[pGuo–H]^-$ that the oxo oxygen atoms of the deprotonated phosphate moiety form strong hydrogen bonds to the hydrogen atom of the 2-amino substituent of the guanine nucleobase and the 3′-hydroxyl hydrogen atom of the sugar moiety. These hydrogen-bonding interactions lead to a *syn* orientation of the nucleobase and C3′-*endo* sugar puckering. The intramolecular hydrogen-bonding interactions with the nucleobase and sugar moieties enhance delocalization of the negative charge on the phosphate moiety. The nucleobase orientation and sugar puckering in $[pdGuo–H]^-$ and $[pGuo–H]^-$ are markedly different from those in $[pdGuo+H]^+$ and $[pGuo+H]^+$, where protonation occurs at the N7 position. The nucleobase exhibits an *anti* orientation as N7 protonation of the guanine nucleobase does not allow it to stabilize the excess charge *via* hydrogen-bonding interactions. Instead, the neutral phosphate moiety is stabilized by a much weaker C8H···O═P noncanonical hydrogen-bonding interaction. The 2′-deoxyribose and ribose sugar moieties prefer C2′-*endo* puckering in the protonated systems. The results found here for $[pdGuo+H]^+$ are consistent with, and therefore further validate, the findings reported by Gidden *et al.*[28] for $[pdGuo+H]^+$ using ion mobility techniques and theory. Thus, the measured collision cross sections, IRMPD spectra, and theory all confirm that protonation induces base rotation in pdGuo, and ensure that the findings indicating base

rotation and changes in the sugar puckering of pdGuo upon protonation are robust. The present results also establish that protonation induced base rotation is not unique to pdGuo, but also occurs for its RNA counterpart, pGuo.

Implications of base flipping of purine nucleotides

The gas-phase conformations of the deprotonated forms of adenine and guanine mononucleotides undergo a change in nucleobase orientation upon protonation.[49] Thus changes in the pH or availability of protons in the local environment can be employed to induce base flipping of the purine nucleobases. Adenine flips from an *anti* (deprotonated) to a *syn* (protonated) orientation,[49] whereas guanine flips from a *syn* (deprotonated) to an *anti* orientation (protonated). This opposing behavior may be a key reason for nature making use of two distinct rather than a single purine nucleobase in nucleic acids. Facile base flipping of the purine nucleobases is consistent with the greater diversity of the purine nucleobase orientations that have been observed in nature than found for the pyrimidine nucleobases. For example, in the common A, B, and Z forms of DNA, the pyrimidine nucleobases exhibit *anti* orientations in all cases, whereas guanine adopts *syn* orientations in the Z-form DNA.[50–52] *Syn* oriented adenine is found to form noncanonical G·A base pairs that lead to changes in both the major and minor grooves of the DNA helix.[53] Guanine nucleobases exhibit *anti* orientations in these G·A (*syn*) base pairs, but exist as an enol–imino tautomer. A close correlation between substitution mutations[54] and the presence of mispairs such as G·A that involve one base in a minor tautomeric form and the other taking on a nucleobase orientation that is opposite that found in Watson–Crick base pairs (*anti*) such that a better understanding of the base flipping behavior of the purine nucleobases is important to understanding and potentially avoiding or correcting genetic mutations.

Conclusions

Comparative analyses of the measured IRMPD and calculated IR spectra in the IR fingerprint and hydrogen-stretching regions suggest that N7 is the most favorable site of protonation for both $[pdGuo+H]^+$ and $[pGuo+H]^+$. The N3 and O6 protonated conformers lie much higher in free energy and are not populated in the experiments, consistent with what is found for $[dGuo+H]^+$ and $[Guo+H]^+$.[33] The IR spectra predicted for various N7 protonated low-energy conformers can be readily distinguished from those of the ground-state **N7A** conformers of $[pdGuo+H]^+$ and $[pGuo+H]^+$ in comparison to the measured IRMPD spectra. The calculated IR spectra for the ground-state **N7A** conformers reproduce the measured spectra quite well. Therefore, the N7 protonated, *anti*-oriented and C2′-*endo* sugar puckered ground-state conformers of $[pdGuo+H]^+$ and $[pGuo+H]^+$ are exclusively populated in the experiments. In contrast, for $[dGuo+H]^+$ and $[Guo+H]^+$,[33] multiple N7 protonated *anti*-oriented low-energy conformers contribute to the experimental population, indicating the importance of the phosphate moiety in limiting the conformational flexibility of the nucleoside building blocks of nucleic acids. The B3LYP relative stabilities of $[pdGuo+H]^+$ and $[pGuo+H]^+$ appear to be more reliable than the MP2(full) results, otherwise several excited low-energy conformers would be expected to be present in the experimental population based on the MP2(full) predicted energetics. The 2′-hydroxyl substituent does not significantly influence the most stable conformations or IRMPD spectral profiles of $[pdGuo+H]^+$ *vs.* $[pGuo+H]^+$, but does however alter the IRMPD yields of $[pdGuo+H]^+$ *vs.* $[pGuo+H]^+$. Clearly, the additional hydrogen-bonding interaction between the 2′- and 3′-hydroxyl substituents influences the efficiency of IVR. The *anti*-oriented and C2′-*endo* sugar puckered most stable conformations of $[pdGuo+H]^+$ and $[pGuo+H]^+$ found here are markedly different from those found for the deprotonated guanine mononucleotides, $[pdGuo-H]^-$ and $[pGuo-H]^-$, in which the deprotonated phosphate moiety is stabilized *via* hydrogen-bonding interactions with both the nucleobase and sugar moieties, rotation of the nucleobase into a *syn* orientation and altering the sugar puckering to C3′-*endo*.[29,30] These contrasting differences suggest that changes in the state of protonation/deprotonation *via* pH changes or the presence of proton donors in the local environment may be employed to induce base rotation and changes in the sugar puckering of guanine nucleotides. Similarly, pH changes also greatly affect the nucleobase orientations of adenine nucleotides, but in the opposite way, adenine rotates from an *anti* to a *syn* orientation upon protonation. Therefore, pH changes may have a great impact on the conformations of purine nucleotides, particularly their nucleobase orientations.

Acknowledgements

Financial support of this work was provided by the National Science Foundation, Grants OISE-0730072, OISE-1357887 and CHE-1409420. R. R. W. also gratefully acknowledges support from a Thomas C. Rumble Graduate Fellowship at Wayne State University. We would also like to thank WSU C&IT for the computational resources and support. This work is part of the research program of FOM, which is financially supported by the Nederlandse Organisatie voor Wetenschappeklijk Onderzoek (NWO). The skillful assistance of J. D. Steill and the FELIX staff is gratefully acknowledged.

References

1 W. Saenger, *Principles of Nucleic Acid Structure*, Springer, New York, 1984.
2 C. Wang, H. Gao, B. L. Gaffney and R. A. Jones, *J. Am. Chem. Soc.*, 1991, **113**, 5468.
3 S. F. Singleton and P. B. Dervan, *Biochemistry*, 1992, **31**, 10995.
4 R. W. Robers and D. M. Crothers, *Proc. Natl. Acad. Sci. U. S. A.*, 1996, **93**, 4320.
5 J. L. Asensio, A. N. Lane, J. Dhesi, S. Bergqvist and T. Brown, *J. Mol. Biol.*, 1998, **275**, 811.

6 A. Rich, *Gene*, 1993, **135**, 99.
7 M. Gueron and J. L. Leroy, *Curr. Opin. Struct. Biol.*, 2000, **10**, 326.
8 S. Neidle and G. N. Parkinson, *Curr. Opin. Struct. Biol.*, 2003, **13**, 275.
9 S. Neidle, *Curr. Opin. Struct. Biol.*, 2009, **19**, 239.
10 L. Ma, M. Lezzi, M. S. Kaucher, Y.-F. Lam and J. T. Davis, *J. Am. Chem. Soc.*, 2006, **128**, 15269.
11 C. Creze, B. Rinaldi, R. Haser, P. Bouvet and P. Gouet, *Acta Crystallogr., Sect. D: Biol. Crystallogr.*, 2007, **63**, 682.
12 D. Kosenkov, L. Gorb, O. V. Shishkin, J. Sponer and J. Leszczynski, *J. Phys. Chem. B*, 2008, **112**, 150.
13 K. Loo, N. Degtyareva, J. Park, B. Sengupta, M. Reddish, C. C. Rogers, A. Bryant and J. T. Petty, *J. Phys. Chem. B*, 2010, **114**, 4320.
14 J.-Y. Salpin, L. MacAleese, F. Chirot and P. Dugourd, *Phys. Chem. Chem. Phys.*, 2014, **16**, 14127.
15 U. Warnke, C. Rappel, H. Meier, C. Kloft, M. Galanski, C. G. Hartinger, B. K. Keppler and U. Jaehde, *ChemBioChem*, 2004, **5**, 1543.
16 B. Chiavarino, M. E. Crestoni, S. Fornarini, D. Scuderi and J.-Y. Salpin, *Inorg. Chem.*, 2015, **54**, 3513.
17 E. O. Hole, W. H. Nelson, E. Sagstuen and D. M. Close, *Radiat. Res.*, 1992, **129**, 119.
18 H. Jurga-Nowak, E. Banachowicz, A. Dobek and A. Patkowski, *J. Phys. Chem. B*, 2004, **108**, 2744.
19 R. Kristelly, G. Gao and J. J. G. Tesmer, *J. Biol. Chem.*, 2004, **279**, 47352.
20 S. Huecas, C. Schaffner-Barbero, W. Garcia, H. Yebenes, J. M. Palacios, J. F. Diaz, M. Menendez and J. M. Andreu, *J. Biol. Chem.*, 2007, **282**, 37515.
21 S. Haider, G. N. Parkinson and S. Neidle, *Biophys. J.*, 2008, **95**, 296.
22 V. Karunakaran, K. Kleinermanns, R. Improta and S. A. Kovalenko, *J. Am. Chem. Soc.*, 2009, **131**, 5839.
23 S. Singh, S. K. Srivastava, P. Donfack, S. Schlucker, A. Materny and B. P. Asthana, *Phys. Chem. Chem. Phys.*, 2012, **14**, 14315.
24 F. Rosu, V. Gabelica, E. De Pauw, R. Antoine, M. Broyer and P. Dugourd, *J. Phys. Chem. A*, 2012, **116**, 5383.
25 A. Ariafard, E. S. Tabatabaie, S. Aghmasheh, S. Najaflo and B. F. Yates, *Inorg. Chem.*, 2012, **51**, 8002.
26 M. R. Ligare, A. M. Rijs, G. Berden, M. Kabelac, D. Nachtigallova, J. Oomens and M. S. de Vries, *J. Phys. Chem. B*, 2015, **119**, 7894.
27 S. Habibi-Goudarzi and S. A. McLuckey, *J. Am. Soc. Mass Spectrom.*, 1995, **6**, 102.
28 J. Gidden and M. T. Bowers, *J. Phys. Chem. B*, 2003, **107**, 12829.
29 Y.-w. Nei, N. Hallowita, J. D. Steill, J. Oomens and M. T. Rodgers, *J. Phys. Chem. A*, 2013, **117**, 1319.
30 Y.-w. Nei, K. T. Crampton, G. Berden, J. Oomens and M. T. Rodgers, *J. Phys. Chem. A*, 2013, **117**, 10634.
31 R. R. Wu, B. Yang, G. Berden, J. Oomens and M. T. Rodgers, *J. Phys. Chem. B*, 2015, **119**, 2795.
32 R. R. Wu, B. Yang, C. E. Frieler, G. Berden, J. Oomens and M. T. Rodgers, *J. Phys. Chem. B*, 2015, **119**, 5773.
33 R. R. Wu, B. Yang, G. Berden, J. Oomens and M. T. Rodgers, *J. Phys. Chem. B*, 2014, **118**, 14774.
34 R. R. Wu, B. Yang, G. Berden, J. Oomens and M. T. Rodgers, *Phys. Chem. Chem. Phys.*, 2016, **17**, 25978.
35 R. R. Wu, B. Yang, G. Berden, J. Oomens and M. T. Rodgers, *J. Am. Soc. Mass Spectrom.*, 2015, **27**, 410.
36 J. J. Valle, J. R. Eyler, J. Oomens, D. T. Moore, A. F. G. van der Meer, G. von Heldon, G. Meijer, C. L. Hendrickson, A. G. Marshall and G. T. Blakney, *Rev. Sci. Instrum.*, 2005, **76**, 023103.
37 N. C. Polfer, J. Oomens, D. T. Moore, G. von Helden, G. Meijer and R. C. Dunbar, *J. Am. Chem. Soc.*, 2006, **128**, 517.
38 N. C. Polfer and J. Oomens, *Phys. Chem. Chem. Phys.*, 2007, **9**, 3804.
39 D. Oepts, A. F. G. van der Meer and P. W. van Amersfoort, *Infrared Phys. Technol.*, 1995, **36**, 297.
40 *HyperChem Computational Chemistry Software Package, Version 5.0*, Hypercube, Inc., Gainsville, FL, 1997.
41 M. J. Frisch, G. W. Trucks, H. B. Schlegel, G. E. Scuseria, M. A. Robb, J. R. Cheeseman, G. Scalmani, V. Barone, B. Mennucci, G. A. Petersson, H. Nakatsuji, M. Caricato, X. Li, H. P. Hratchian, A. F. Izmaylov, J. Bloino, G. Zheng, J. L. Sonnenberg, M. Hada, M. Ehara, K. Toyota, R. Fukuda, J. Hasegawa, M. Ishida, T. Nakajima, Y. Honda, O. Kitao, H. Nakai, T. Vreven, J. A. Montgomery, Jr., J. E. Peralta, F. Ogliaro, M. Bearpark, J. J. Heyd, E. Brothers, K. N. Kudin, V. N. Staroverov, R. Kobayashi, J. Normand, K. Raghavachari, A. Rendell, J. C. Burant, S. S. Iyengar, J. Tomasi, M. Cossi, N. Rega, J. M. Millam, M. Klene, J. E. Knox, J. B. Cross, V. Bakken, C. Adamo, J. Jaramillo, R. Gomperts, R. E. Stratmann, O. Yazyev, A. J. Austin, R. Cammi, C. Pomelli, J. W. Ochterski, R. L. Martin, K. Morokuma, V. G. Zakrzewski, G. A. Voth, P. Salvador, J. J. Dannenberg, S. Dapprich, A. D. Daniels, Ö. Farkas, J. B. Foresman, J. V. Ortiz, J. Cioslowski and D. J. Fox, *Gaussian 09, Revision C.01*, Gaussian, Inc., Wallingford, CT, 2009.
42 S. Katsyuba and E. Vandyukova, *Chem. Phys. Lett.*, 2003, **377**, 658.
43 J. O. Jensen, A. Banerjee, D. Zeroka, C. N. Merrow, S. J. Gilliam and S. J. Kirkby, *Spectrochim. Acta, Part A*, 2004, **60**, 1947.
44 D. Scuderi, C. F. Correia, O. P. Balaj, G. Ohanessian, J. Lemaire and P. Maitre, *ChemPhysChem*, 2009, **10**, 1630.
45 B. S. Fales, N. O. Fujamade, Y.-w. Nei, J. Oomens and M. T. Rodgers, *J. Am. Soc. Mass Spectrom.*, 2011, **22**, 81.
46 B. S. Fales, N. O. Fujamade, J. Oomens and M. T. Rodgers, *J. Am. Soc. Mass Spectrom.*, 2011, **22**, 1862.
47 J. R. Eyler, *Mass Spectrom. Rev.*, 2009, **28**, 448.

48 J. Oomens and N. C. Polfer, *Mass Spectrom. Rev.*, 2009, **28**, 468.
49 R. R. Wu, C. C. He, L. A. Hamlow, Y.-w. Nei, G. Berden, J. Oomens and M. T. Rodgers, *J. Phys. Chem. B*, 2016, DOI: 10.1021/acs.jpcb.6b04052.
50 R. R. Sinden, *DNA Structure and Function*, Academic Press, 1994.
51 A. Rich, A. Norheim and A. H. J. Wang, *Annu. Rev. Biochem.*, 1984, **53**, 791.
52 P. S. Ho, *Proc. Natl. Acad. Sci. U. S. A.*, 1994, **91**, 9549.
53 T. Brown, W. N. Hunter, G. Kneale and O. Kennard, *Proc. Natl. Acad. Sci. U. S. A.*, 1986, **83**, 2402.
54 M. D. Topal and J. R. Fresco, *Nature*, 1976, **263**, 285.